12TH INTERNATIONAL SYMPOSIUM ON FLOW VISUALIZATION
September 10-14, 2006, German Aerospace Center (DLR), Göttingen, Germany
doi: 10.5281/zenodo.14845

A NOVEL METHOD FOR SPATIOTEMPORAL ANALYSIS OF FLOWS WITHIN THE WATER-SIDE VISCOUS BOUNDARY LAYER

Markus Jehle, Bernd Jähne
Interdisciplinary Center for Scientific Computing (IWR), University of Heidelberg;
Institute for Environmental Physics (IUP), University of Heidelberg

Keywords: *optical flow, image processing, fluid flow analysis, boundary layer*

ABSTRACT

A novel measurement technique is developed for 3D reconstruction of Eulerian velocity vector fields and Lagrangian trajectories at water-side viscous boundary layers in wavy free surfaces. The presented approach makes use of spatiotemporal image processing algorithms. The method is applied to a falling film with a known velocity profile.

1 INTRODUCTION

In order to examine the air-water gas exchange, a detailed knowledge is needed of the flow field within the water-side viscous boundary layer. For review articles about the mechanisms of gas transfer we refer to [2],[7]. Therefore, important quantities, such as shear stresses, velocity profiles, dissipation rates, and Lagrangian trajectories, have to be determined.

The measurement technique has to fulfil following requirements:

- The interesting flow is inherently 3D: Interesting features of the flow are (microscale-) wave-breaking, (micro-) Langmuir circulations and turbulence. All of these have in common, that they are three-dimensional phenomena. A classical measurement setup, like Particle Image Velocimetry (PIV) [12], which uses laser light sections, yields only a slice of the flow-field and suppresses its three-dimensionality. For examples of 2D-measurements we relate exemplarily to [9], [10], and [11].

- We are interested in the flow inside the water-side viscous boundary layer, which is of thickness $O(1\,\mathrm{mm})$. In contrast to that, waves may have amplitudes of $O(10\,\mathrm{cm})$. Because of this discrepance, it is hardly possible, to observe the flow field statically from the side, which would be a necessary condition of using laser light sections. Either, we have to use a sophisticated wave tracking mechanism, or we have to look from above, perpendicular to the water surface.

- Waves and turbulence are instationary processes. Because in this case the Lagrangian path lines are different from the Eulerian stream lines, it is not sufficient, to reconstruct the flow field taking

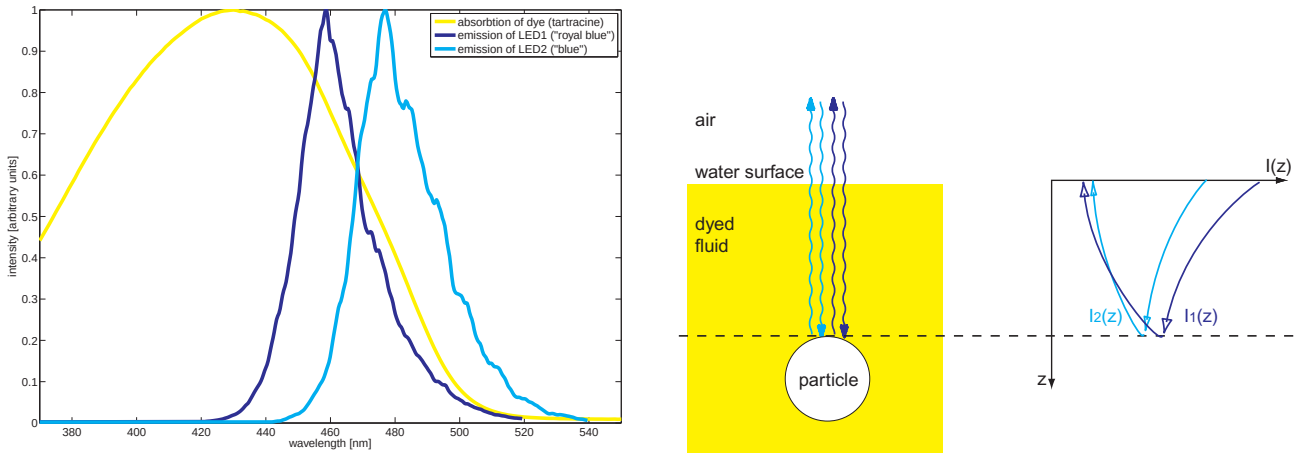

Fig. 1 Left: The emitted light of the two types of LEDs ("blue" and "royal blue") is absorbed unequally by the dye (tartrazine acid yellow). Right: Sketch of the principle.

two images, like it is realized in classical PIV. We have to track particles in an image sequence. In our approach we are not only capable to record time resolved data, but also we make use of its spatiotemporal structure, which is a great advantage over correlation based-techniques, like PIV.

A technique similar to the one proposed here is applied successfully in the field of biofluidmechanics, where it is important to acquire knowledge about the flow in (artificial) blood vessels [4].

The next sextion is concerned with the basic principles of our measurement technique. Both, the reconstruction of the 3D-position and of the three-component velocity of the tracer particles representing the flow will be addressed. In order to realize these ideas, we had to design a new measurement setup, and we had to implement the algorithmics, which will be addressed in sections 3 and 4. First results are given in section 5. We complete our paper with a conclusion and an outlook.

2 METHOD

A fluid volume is illuminated by LEDs. Small hollow glass spheres (mean diameter 30 μm) are added to the fluid, functioning as a tracer. A high speed camera pointing to the water surface from above records the image sequences. A dye, namely tartracine acid yellow, is added to the fluid, which limits the penetration depth of the light into the flow model acoording to Beer-Lambert's Law:

$$I_p(z) = I_0 \exp -z/\tilde{z}_*,$$

where $I_p(z)$ is the intensity of the light approaching the particle, which is located at a depth z from the surface, I_0 is the light's intensity before penetrating the fluid and $\tilde{z}_*$ is the penetration depth. The light is reflected by the glass sphere, and passes the distance z again, before approaching the wall with the intensity

$$I(z) = I_p(z) \exp -z/\tilde{z}_* = I_0 \exp -2z/\tilde{z}_* = I_0 \exp -z/z_*,$$

where we have introduced an effective penetration depth $z_* = \tilde{z}_*/2$ for convenience. Within the illuminated layer the particles appear more or less bright, depending on their normal distance to the wall: Particles near the wall appear brighter, i. e. have a higher gray value than particles farther away from the wall. Because the diameter of the spheres is considerably greater than the wavelength of the light, we are in the geometric scattering range, and can neglect Mie effects.

The particle's intensity $I(z)$ is mapped to a grayvalue $g(I(z))$ by the procedure of imaging. For simplicity, we assume, that the response of the camera is linear, i. e., we are allowed to write

$$g(z) = g_0 \exp -z/z_*. \tag{1}$$

Estimating the depth In order to eliminate the depth z in equation (1) we have to know g_0. If all particles are of the same type (size, reflectance, etc.), then we obtain g_0 by means of calibration. In our situation this is not possible, because we use heterodisperse particles, i. e. particles, which have a broad distribution in size. Therefore, we illuminate the fluid alternately with LEDs of two different spectra (see figure 1). We choose the maxima of the spectral bands to 455 nm ("royal blue"), and to 470 nm ("blue"). The light of each LED is absorbed by the dye in a different manner, which can be expressed by the effective penetration depths: z_{*1} for the first LED-type and z_{*2} for the second LED-type. z_{*1} and z_{*2} can be measured using a spectrometer, for instance. We write down Beer-Lambert's law for each kind of LED-type:

$$g_1(z) = g_{01} \exp -z/z_{*1} \quad \text{and} \quad g_2(z) = g_{02} \exp -z/z_{*2}.$$

We solve this equation system for the depth of the particle:

$$z(g_1, g_2) = \frac{z_{*1} z_{*2}}{z_{*1} - z_{*2}} \left(\ln\left(\frac{g_1}{g_2}\right) + \ln\left(\frac{g_{02}}{g_{01}}\right) \right). \tag{2}$$

Note, that here the depth of the particle merely depends on the ratio of the intensities g_{01}/g_{02}, which is for all particles the same, and which can be calibrated.

Estimating the velocities The velocity vectors of the flow are obtained by an extension of the method of optical flow, therefore allowing for changes in exponential brightness [5]. We differentiate equation (1) with respect to t:

$$\frac{\mathrm{d}g}{\mathrm{d}t} = -\frac{g_0}{z_*}\frac{\mathrm{d}z}{\mathrm{d}t} \exp -z/z_* = -\frac{1}{z_*}\frac{\mathrm{d}z}{\mathrm{d}t} g = -\frac{w}{z_*} g,$$

where we have introduced $w = \mathrm{d}z/\mathrm{d}t$, the component of the particle's velocity perpendicular to the wall. Because we can express the total derivative of the gray value g using the chainrule

$$\frac{\mathrm{d}g}{\mathrm{d}t} = \frac{\partial x}{\partial t}\frac{\partial g}{\partial x} + \frac{\partial y}{\partial t}\frac{\partial g}{\partial y} + \frac{\partial g}{\partial t} = u\frac{\partial g}{\partial x} + v\frac{\partial g}{\partial y} + \frac{\partial g}{\partial t},$$

we arrive at a partial differential equation for three unknows $(u, v, w)^T$, given the spatiotemporal gradient $(\partial g/\partial x, \partial g/\partial y, \partial g/\partial t)^T$ of the flow, and the gray value itself:

$$u\frac{\partial g}{\partial x} + v\frac{\partial g}{\partial y} + \frac{\partial g}{\partial t} + w\frac{g}{z_*} = 0. \tag{3}$$

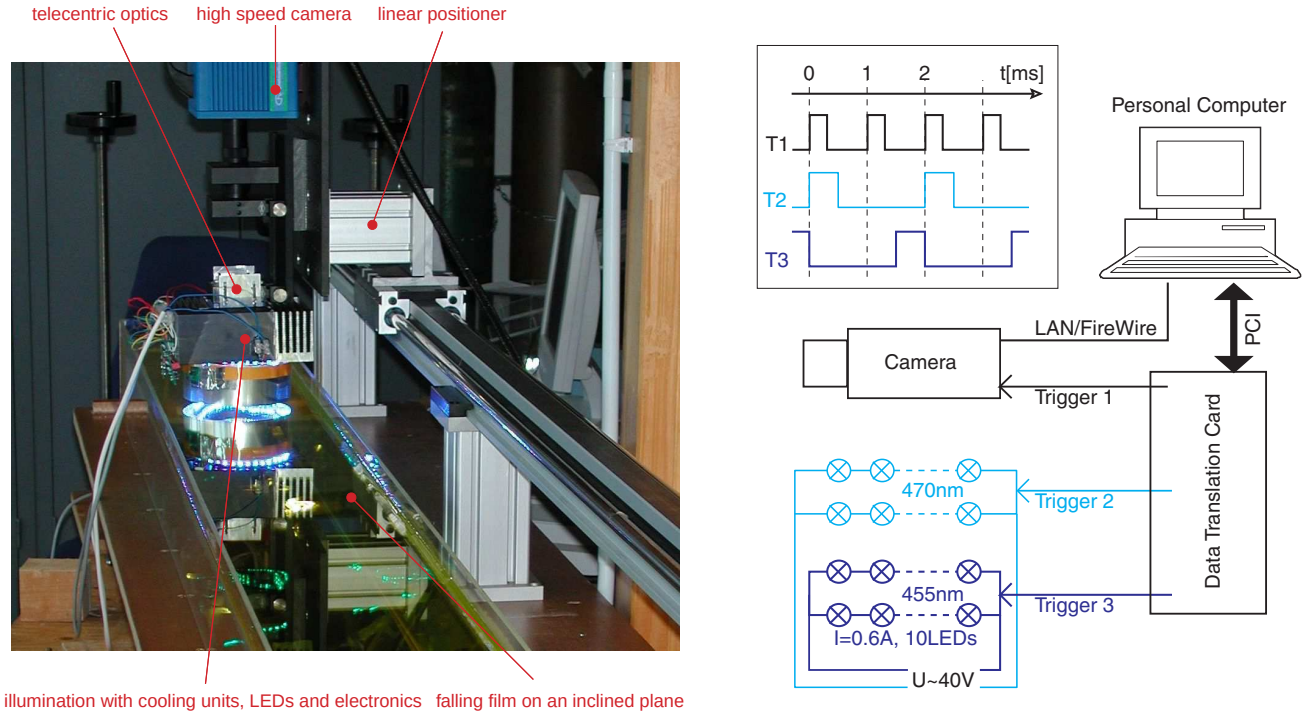

Fig. 2 Left: Experimental setup, designed for measurements in a free falling film. Right: Triggering of the illumination unit and of the camera

This can be rewritten to a scalar-product of data- and parameter vector:

$$\vec{d} \times \vec{p}^T = \left(\frac{\partial g}{\partial x}, \frac{\partial g}{\partial y}, \frac{g}{z_*}, \frac{\partial g}{\partial t} \right) \times (u, v, w, 1)^T = 0.$$

We solve this equation, using data in a spatiotemporal neighborhood about the point, where we want to estimate the velocity field, by applying a total-least-squares-estimator. For details we refer to [8].

3 MEASUREMENT SETUP

The measurement setup, designed for measurements in a free falling film, is displayed in figure 2, left. We use a high speed camera with a back-illuminated CCD-sensor, to achieve a high quantum efficiency in the spectral band of interest. It is capable of acquiring 1000 frames per second at a resolution of 512×512 pixels[2]. Because we require, that the lateral object size is independent from the longitudinal distance from the camera, we installed a telecentric optics. Figure 2, right, shows schematically the triggering of the illumination setup and of the camera. In the box on the top left of this figure a possible triggering schedule is presented. For illumination we chose 2×20 powerful Luxeon III Emitter LEDs[1], because they supply a luminous flux of about 20 lm at a current of 600 mA (operating at a voltage of

[1] http://www.lumileds.com/pdfs/DS45.PDF

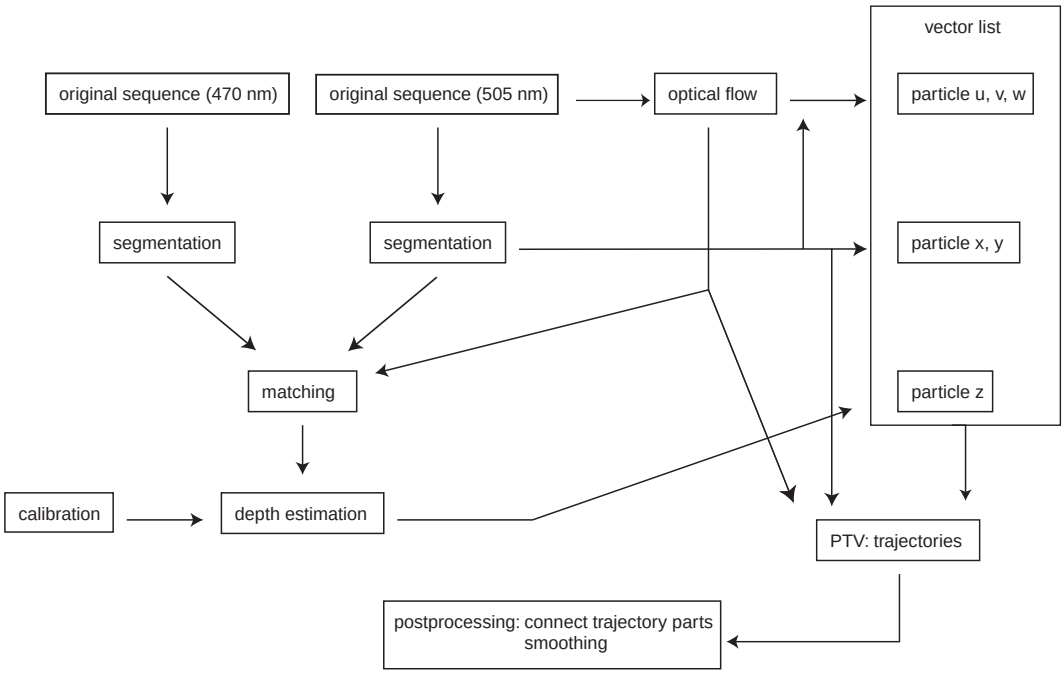

Fig. 3 Image processing procedure (description in text).

about 4 V), and are available in the desired spectral ranges. Before mounting we had to sort the LEDs, because due to the manifacturing process they differ in their output spectra. We installed a passive cooling, which was capable to transport the emerging heat of about 30 W outwards.

4 IMAGE PROCESSING

The image processing procedure is displayed in figure 3. The acquired images undergo a radiometric calibration, which compensates for the nonlinearity of the CCD-chip response, and for the inhomogenity of the sensor array, which is essentially composed of eight individually amplified sections. Then we perform an illumination correction on each image of the sequence individually by dividing the image by its low-pass-filtered version.

For determing the position of the particles, and for getting the brightness of the particles, they have to be segmented. In order to do this, we apply the region-growing algorithm, which is described in [6] in detail. It is based on searching for the local maxima in the image, and then subsequently adding adjacent pixels using prior information of the shape of a typical particle (area, excentricity), and of the image noise. For the brightness of a particle we use its maximum grayvalue. We have done experiments, using the integral of the grayvalue over the whole particle, and applying a gaussian fit, but we didn't find any improvements in accuracy compared to the maximum grayvalue.

We determine the velocity vector applying model equation (3). Our total-least-squares estimator yields - besides the velocity vector itself - a confidence measure, so we only get velocity information,

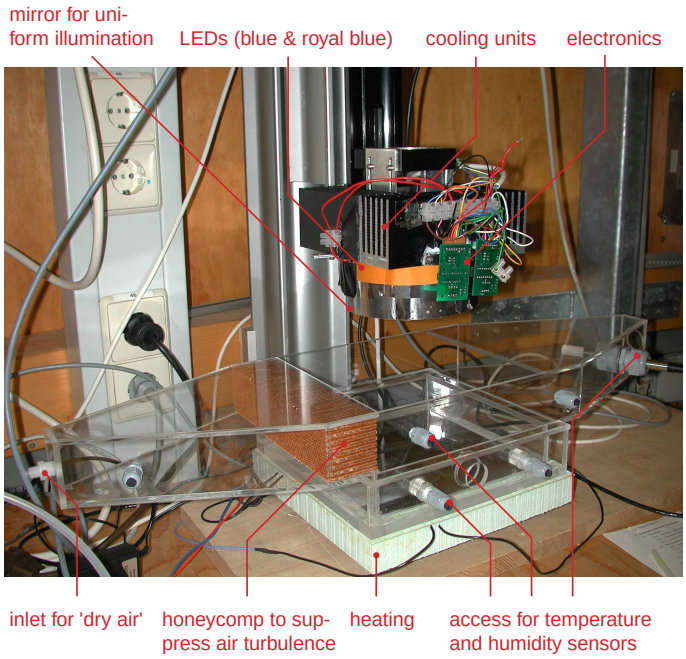

Fig. 4 Setup of the convection tank experiment

where a reliable estimation is possible. At places, where no unambiguous fit to equation (3) is possible, we cannot specify a velocity vector. This occurs at the presence of multiple motions inside the spatiotemporal neighborhood.

For the calculation of the depth z of a particle according to equation (2) we need the maximum grayvalues of one and the same same particle, recorded at 455 nm and recorded at 470 nm. Because the LEDS are triggered successively, the particle undergoes a displacement between the two recordings. We have to find correspondences of the same particle between one image and the other. To minimize the search radius, we warp one image against the other, using the previously determined velocity vector field. Using the same procedure, we find particle trajectories, which extend accross more than to images. A similar technique is described in [3], where PIV information is used to improve Particle Tracking.

By combining the information about position (x,y,z) and velocity (u,v,w), an irregularily sampled 3D3C-Eulerian velocity vector field is at hand. We can use some kind of interpolation schemes (for example the Adaptive Gaussian Windowing method presented in [1]) to obtain a dense motion field from which we are able to calculate derived quantities, like shear rates and vorticity.

An alternative is the Lagrangian representation, which has become feasible, because we obtained particle trajectories, which represent the path lines of the flow. It is suitable for visualizing instationary flows.

5 RESULTS

We have applied the technique for measurements in a convection tank and in a falling film. For the purpose of this paper, the convection-tank-measurements are just for qualititive illustration of the feasi-

bility of our method, whereas the measurements in the falling film can be compared with the analytical solution of the flow, so that we have some kind of “ground truth”.

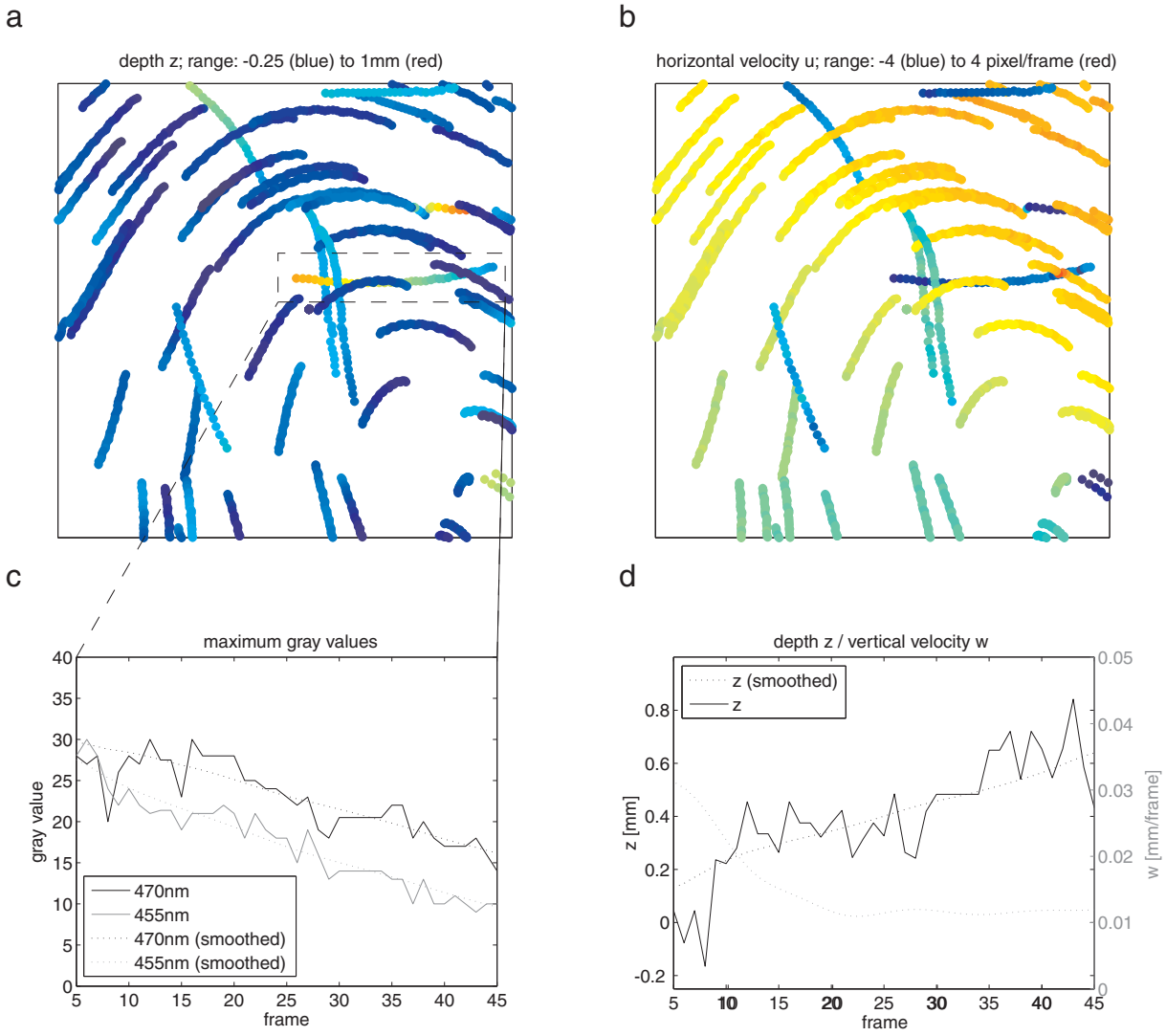

Fig. 5 An example of a typical convective flow. a) Flow trajectories, depth is colorcoded. b) Flow trajectories, horizontal velocities are colorcoded. c) Time series of maximum grayvalues of one trajectory. d) Time series of depth z and of vertical velocity w of the same trajectory

Buoyant convective turbulence We chose buoyant convective turbulence for demonstrating our technique, because it exhibits a truely three-dimensional flow. Because the flow is moderate in velocity (flow speeds of less than 1 cm/s), we can use a camera with a high-quality, high-resolution sensor operating at a frame rate of 30 frames per second.

The setup of the convection tank experiment is shown in figure 4. The fluid is put in a rectangular volume of dimensions $20 \times 20 \times 5$ cm^3, and is heated from below with a heating power of about 50 W.

Cool, dry air is directed across the fluid to transport the developing moisture. The flow parameters are monitored using temperature and humidity sensors.

An exemplary analysis is shown in figure 5. The complex structure of the flow is reproduced in the analysis. While most of the tracer particles at the top describe a vortex-like structure, some particles, which are situated in deeper regions, move in different directions.

Having a closer look to one of the trajectories, we find, that while the particle dives down into the fluid, i. e. it's z-coordinate gets larger, it's velocity $w = \partial z/\partial t$ remains positive. Note, that w is calculated, using the model 3, i. e. directly from the image sequence, and *not* with the aid of the calculated z-coordinates.

From figures 5 c) and d) we find, that the maximum grayvalue of a particle exhibits strong fluctuations while moving along a trajectory. This is due to the fact, that the particle, whose imaged size is typically about 3 pixels in diameter, moves continuously across the pixels of the sensor; the maximum gray value depends on its sub-pixel-position. This effect has the same origin, like "peak locking" in PIV [12]. In our application its impact is even more dramatic, because we use itensity data in a direct way. Assuming a continuous progression of a particle, we are allowed to smooth the maximum gray values along one trajectory (e. g. using a low-pass-filter), which results in a smooth behaviour of the depth z along a trajectory.

Laminar falling film In order to quantify our measurement technique, we chose a flow, for which we can easily write down an analytical solution. The flow down an inlinced plane, commonly referred to as "falling film". In the regime of moderate Reynolds numbers, v and w vanish, and u depends only on z in the way

$$u(z) = \frac{g \sin\alpha}{2\nu}(d^2 - z^2) \quad \text{with} \quad d = \sqrt[3]{\frac{3\nu Q}{bg\sin\alpha}},$$

where g denotes the gravitational constant, α is the inclination of the plane, ν is the kinematic viscosity, Q is the throughput, b is the width, and d is the thickness of the flow. The velocity profile describes a parabola. For an illustration, see figure 6. By tuning the external parameters α, ν, Q, and d we can control the flow thickness d and moreover its maximum velocity $u(z = 0)$.

Figure 5 shows an example of an obtained velocity-profile. Note, that, because the particles move from right to left, the horizontal velocity is negative. Because the flow is stationary, we averaged the u in z-windows of width 50 μm. The results can be fitted with a theoretically predicted parabola very well.

6 CONCLUSION AND FURTHER WORK

A novel particle-based technique for 3D3C-fluid flow measurement is presented, which is suited for the investigation of boundary layers at free surfaces. By coding the depth of the particles supplementing a dye, we are able to reconstruct its 3D-position using one single camera. Using an optical-flow-based procedure for velocity analysis, we are capable of determining the three components of the particle's velocity. This is possible, because we take the change of the brightness of an imaged particle as the velocity component perpendicular to the image plane. We applied our method to the cases of buoyant convective turbulence and a laminar falling film.

We plan to verify the measurements using infrared-thermography. Moreover we will set up our experiment in a linear wind-wave-tunnel, to examine the case of wind-driven shear flow. Using an

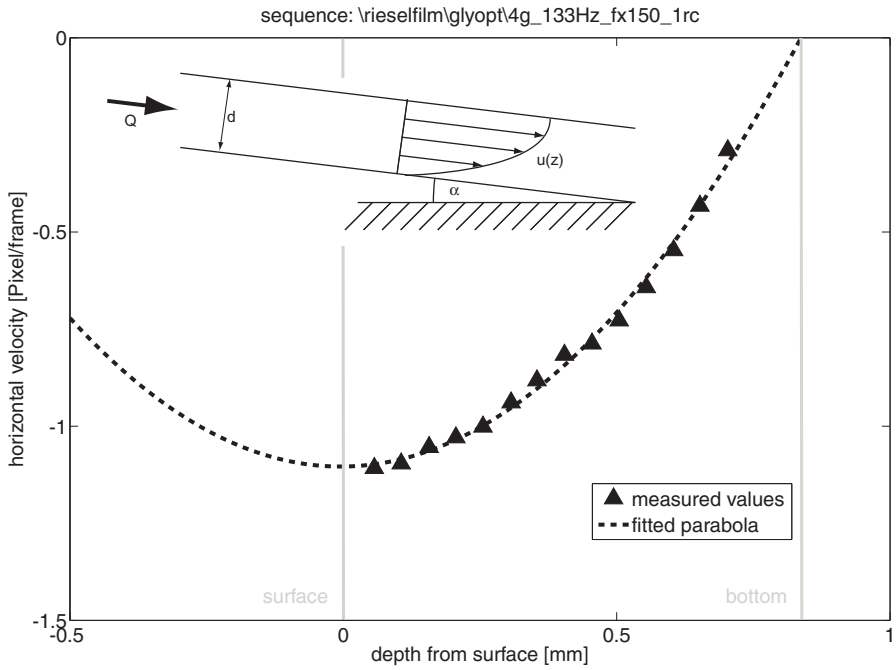

Fig. 6 Left: Experimental setup, designed for measurements in a free falling film. Right: Triggering of the illumination unit and of the camera

imaging slope gauge, we can simultaneously quantify the slope of the waves, so that we can adopt our measuring technique to wavy, free surfaces.

Acknowledgements We gratefully acknowledge the support by the priority program 1147 of the German Research Foundation.

REFERENCES

[1] J. C. Agüi and J. Jimenez. On the performance of particle tracking. *Journal of Fluid Mechanics*, 185:261–304, 1987.

[2] S. Bannerjee and S. MacIntyre. The air-water interface: Turbulence and scalar interchange. In P. L. F. Liu, ed., *Advances in Coastal and Ocean Engineering*, vol. 9, pp. 181–237. World Scientific, Hackensack, N. J., 2004.

[3] E. Cowen and S. Monismith. A hybrid digital particle tracking velocimetry technique. *Experiments in Fluids*, 22:199–211, 1997.

[4] P. Debaene. *Neuartige Messmethode zur zeitlichen und örtlichen Erfassung der wandnahen Strömung in der Biofluidmechanik.* Phd thesis, TU Berlin, 2005.

[5] H. W. Haussecker and D. J. Fleet. Computing Optical Flow with Physical Models of Brightness Variation. *PAMI*, 23(6):661–673, 2001.

[6] F. Hering. *Lagrangesche Untersuchungen des Strömungsfeldes unterhalb der wellenbewegten Wasseroberfläche mittels Bildfolgenanalyse*. PhD thesis, University of Heidelberg, 1996.

[7] B. Jähne and H. Haußecker. Air-water gas exchange. *Annual review of Fluid Mechanics*, 30, 1998.

[8] M. Jehle and B. Jähne. Direct estimation of the wall shear rate using parametric motion models in 3D. In *Pattern Recognition, 28th DAGM*, 2006.

[9] W. K. Melville, R. Shear, and F. Veron. Laboratory measurements of the generation and evolution of Langmuir circulations. *Journal of Fluid Mechanics*, 364:31–58, 1998.

[10] K. Okuda. Internal flow structure of short wind waves, Part I. On the Internal Vorticity Structure. *Journal of the Oceanographical Society of Japan*, pp. 28–42, 1982.

[11] W. L. Peirson and M. L. Banner. Aqueous surface layer flows induced by microscale breaking wind waves. *Journal of Fluid Mechanics*, 479:1–38, 2003.

[12] M. Raffel, C. Willert, and J. Kompenhans. *Particle Image Velocimetry. A Practical Guide.* Springer, Berlin, Heidelberg, New York, 1998.